Supporting Information

Neodymium-based B-site high-entropy perovskite oxide nanoparticles as an efficient electrocatalyst for water splitting and methanol oxidation

Zohreh Shaghaghi[a, *], Mehri Aligholivand [a], and Alireza Khataee [b,c]

[a] *Coordination Chemistry Research Laboratory, Department of Chemistry, Faculty of Basic Sciences, Azarbaijan Shahid Madani University, Tabriz, Iran*

[b] *Department of Applied Chemistry, Faculty of Chemistry, University of Tabriz, 51666-16471, Tabriz, Iran*

[c] *Department of Chemical Engineering & ITU Synthetic Fuels and Chemicals Technology Center (ITU-SENTEK), Istanbul Technical University, Istanbul 34469, Türkiy*

** Corresponding author: shaghaghi@azaruniv.ac.ir, zsh024@gmail.com*

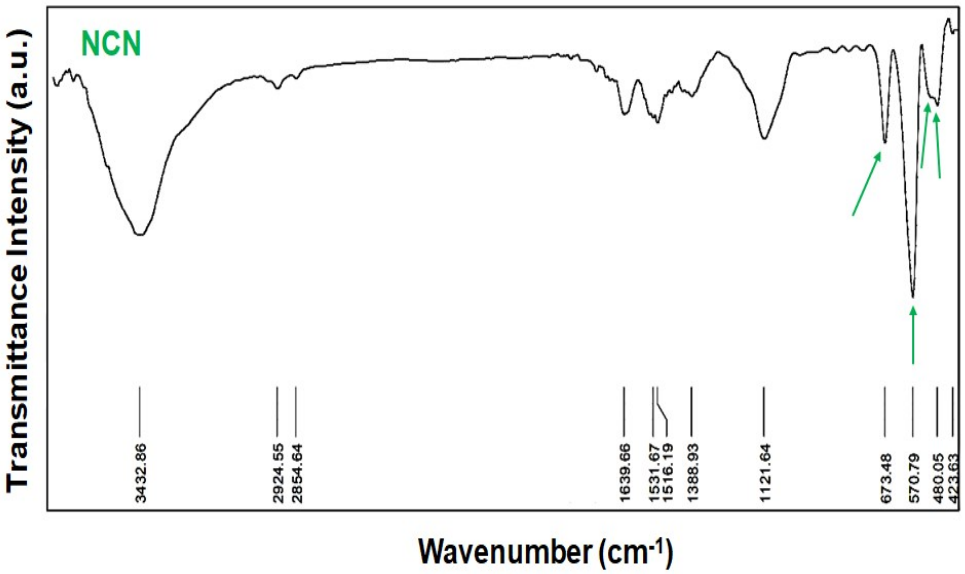

Fig. S1. FTIR spectrum of $Nd(CoNi)O_{3-\delta}$ (NCN).

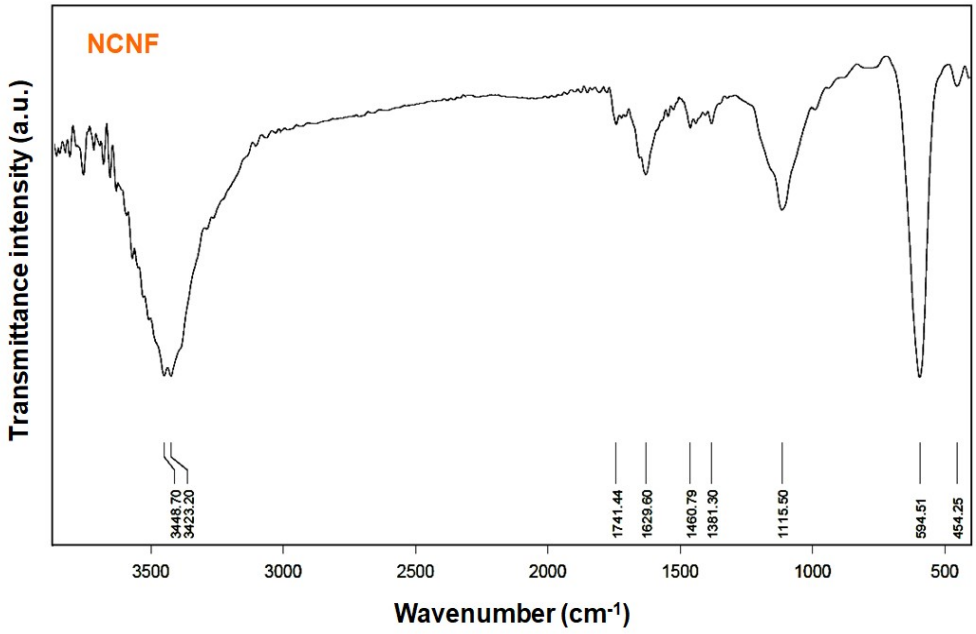

Fig. S2. FTIR spectrum of $Nd(CoNiFe)O_{3-\delta}$ (NCNF).

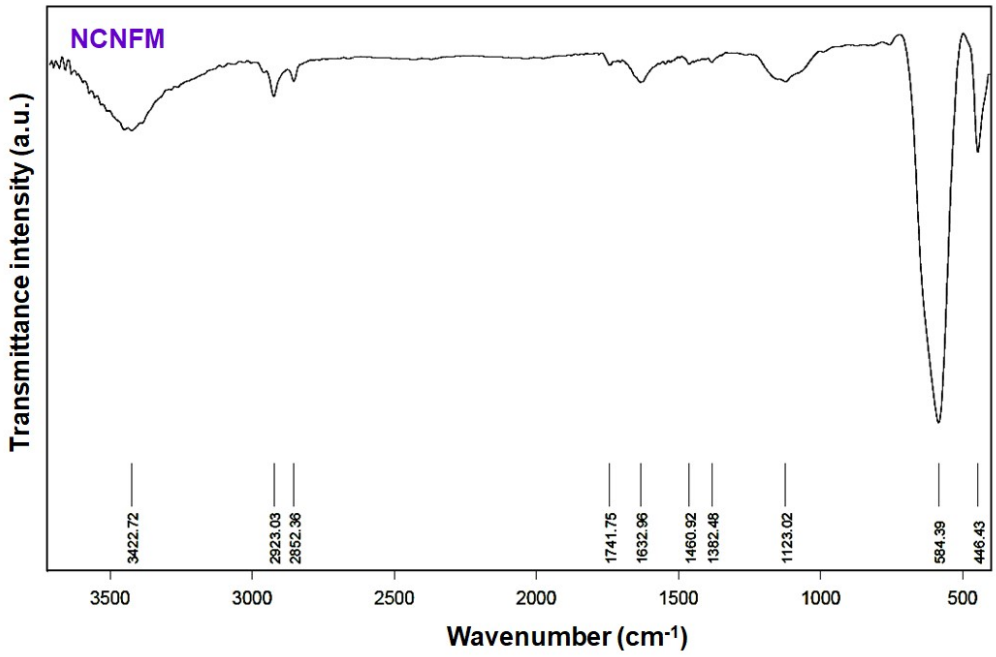

Fig. S3. FTIR spectrum of Nd(CoNiFeMn)$O_{3-\delta}$ (NCNFM).

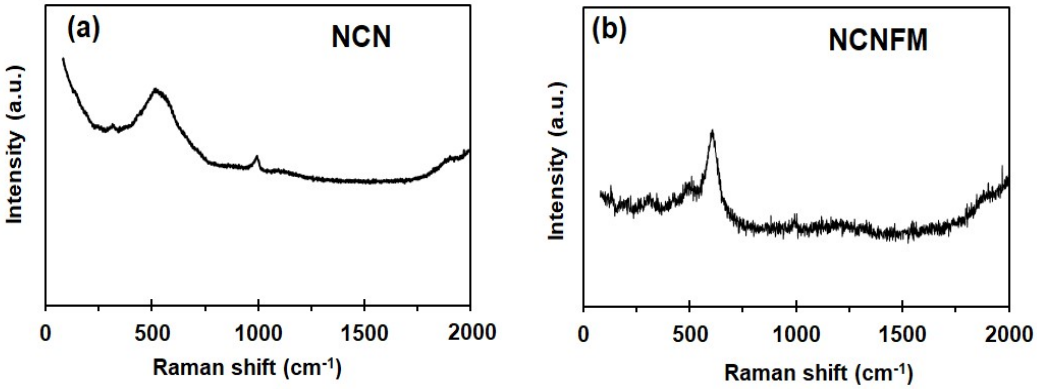

Fig. S4. Raman spectra of Nd(CoNi)$O_{3-\delta}$ (NCN) (a) and Nd(CoNiFeMn)$O_{3-\delta}$ (NCNFM) (b)

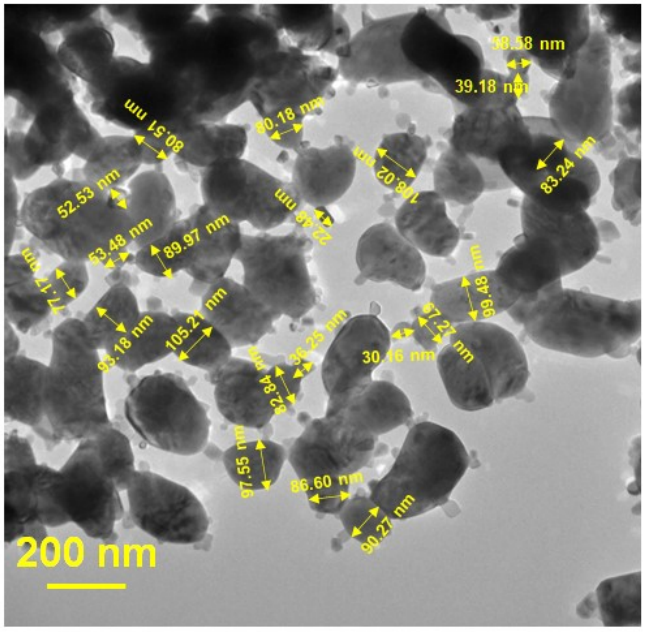

Fig. S5. HRTEM image of the NCNFM perovskite.

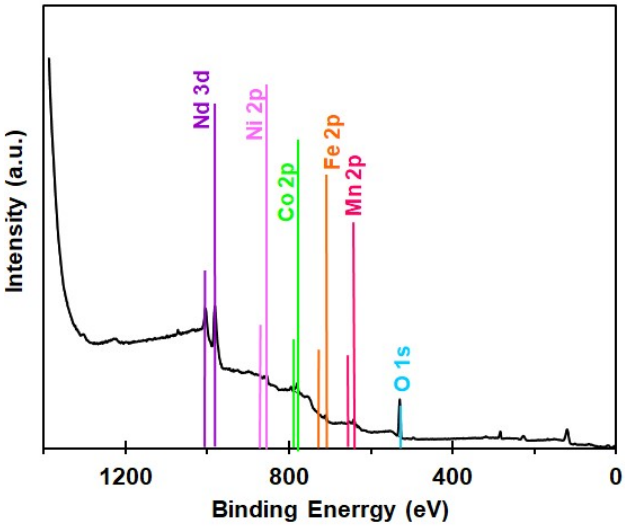

Fig. S6. The survey XPS spectrum of NCNFM.

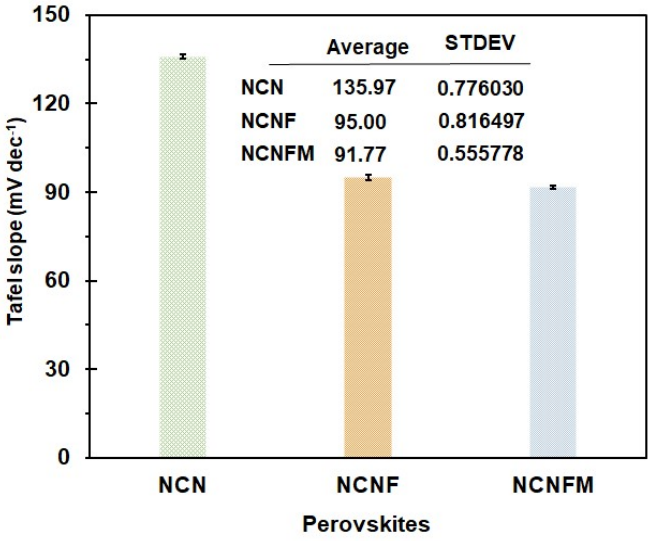

Fig. S7. Bar diagrams with error bars, showing Tafel slope values for catalysts in OER.

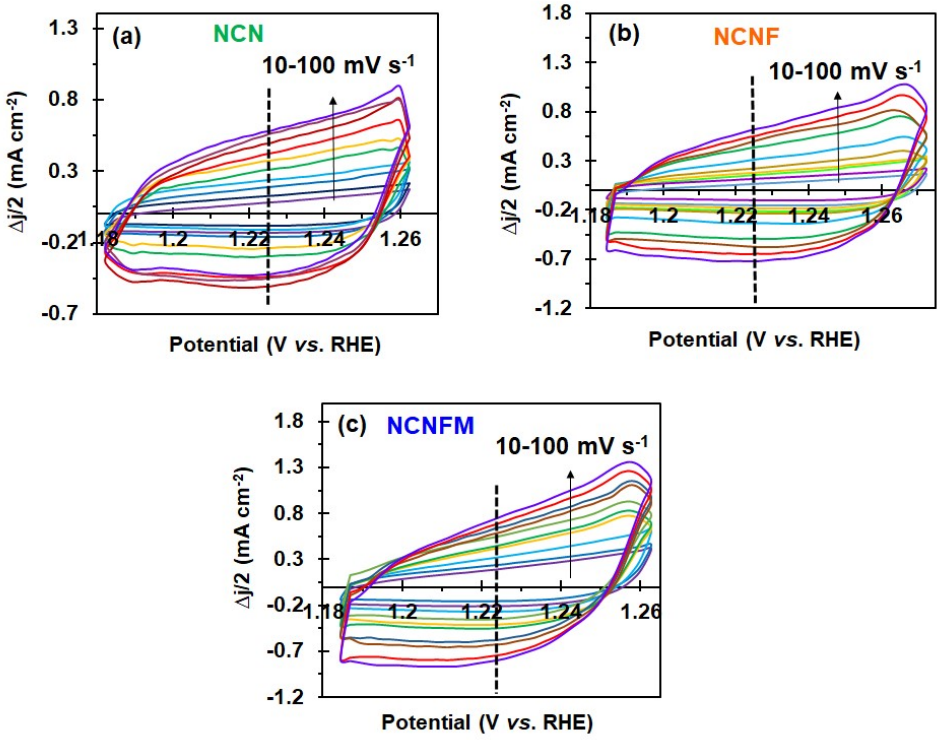

Fig. S8. CVs for NCN (a), NCNF (b), and NCNFM (c) at different scan rates within non-faradaic regions in 1.0 M KOH electrolyte.

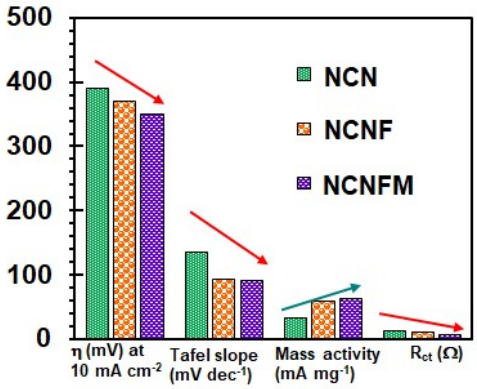

Fig. S9. Comparison of the OER activity of the NCN, NCNF, and NCNFM electrocatalysts.

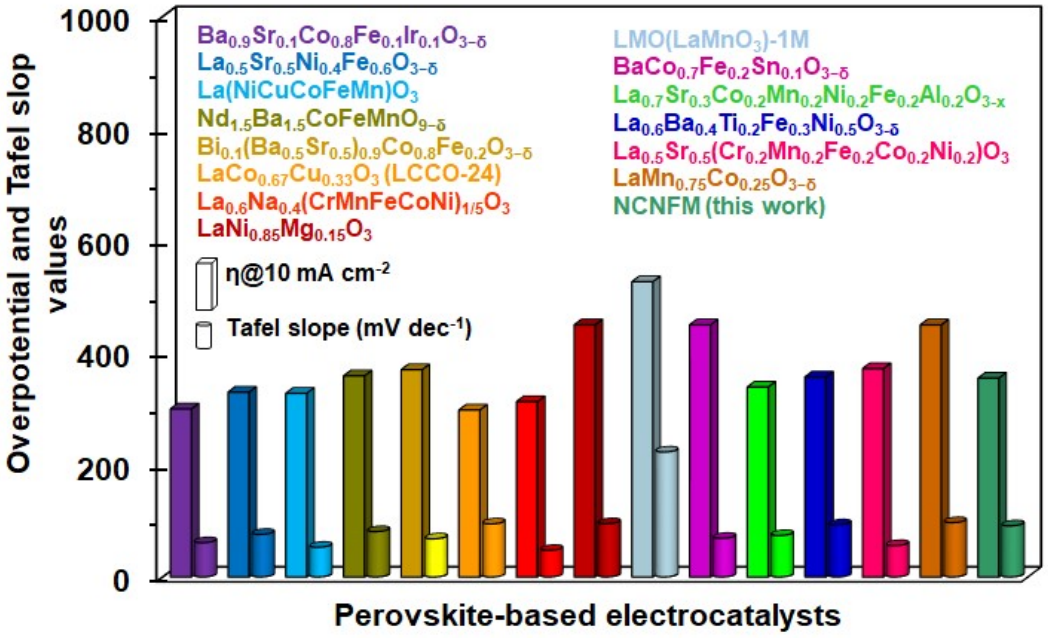

Fig. S10. Comparison of the OER activity of the NCNFM perovskite with some previous reported high-entropy perovskites [1-14].

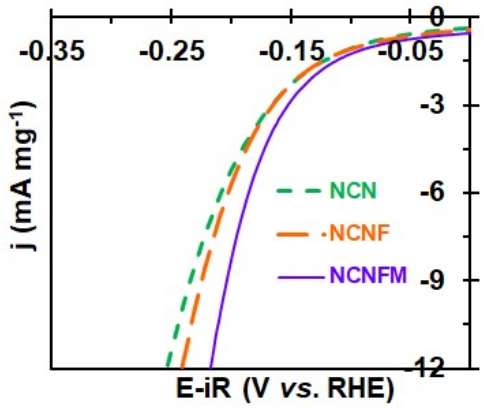

Fig. S11. Normalized LSV curves, showing mass activity in HER for electrocatalysts.

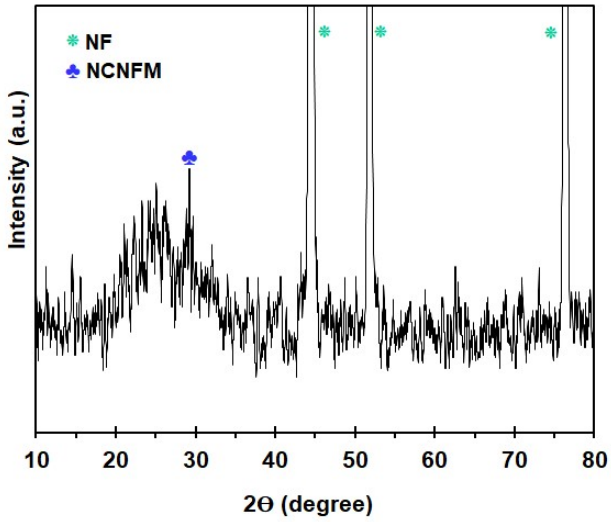

Fig. S12. PXRD pattern of the surface of modified NF with NCNFM after performing the CP test for HER.

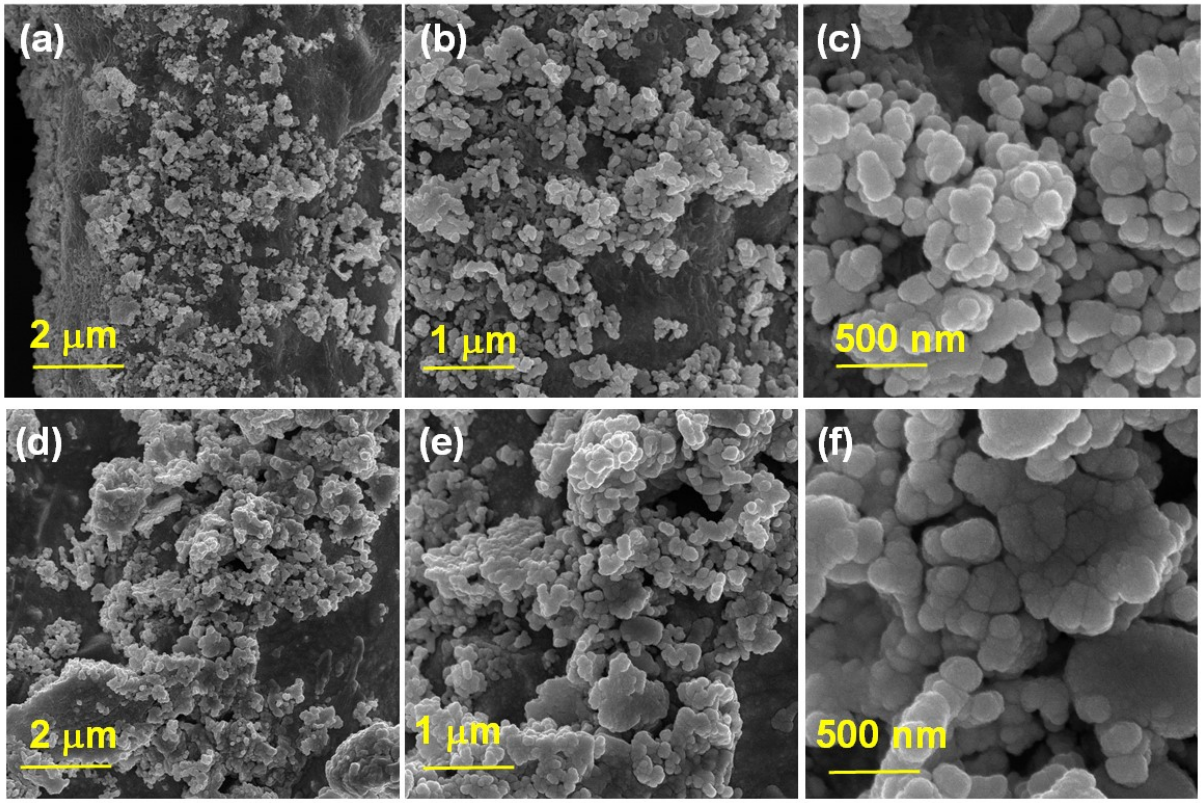

Fig. S13. FE-SEM images of the surface of modified NF with NCNFM before (a, b, and c) and after (d, e, and f) performing the CP test for HER.

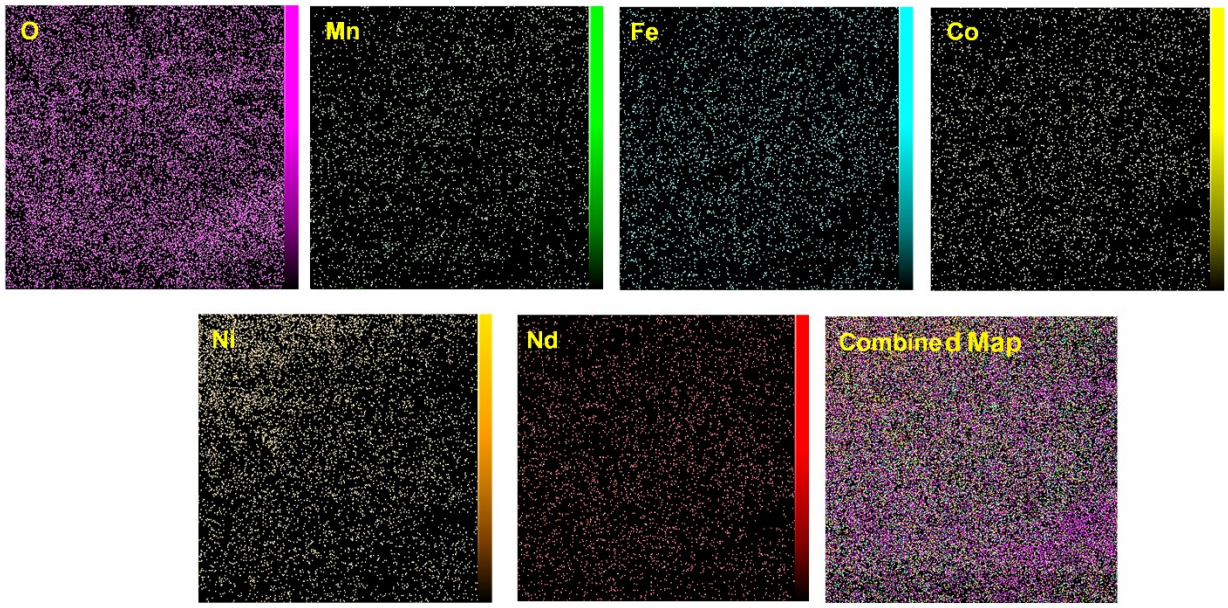

Fig. S14. FE-SEM/EDX images of the surface of modified NF with NCNFM before performing the CP test for HER.

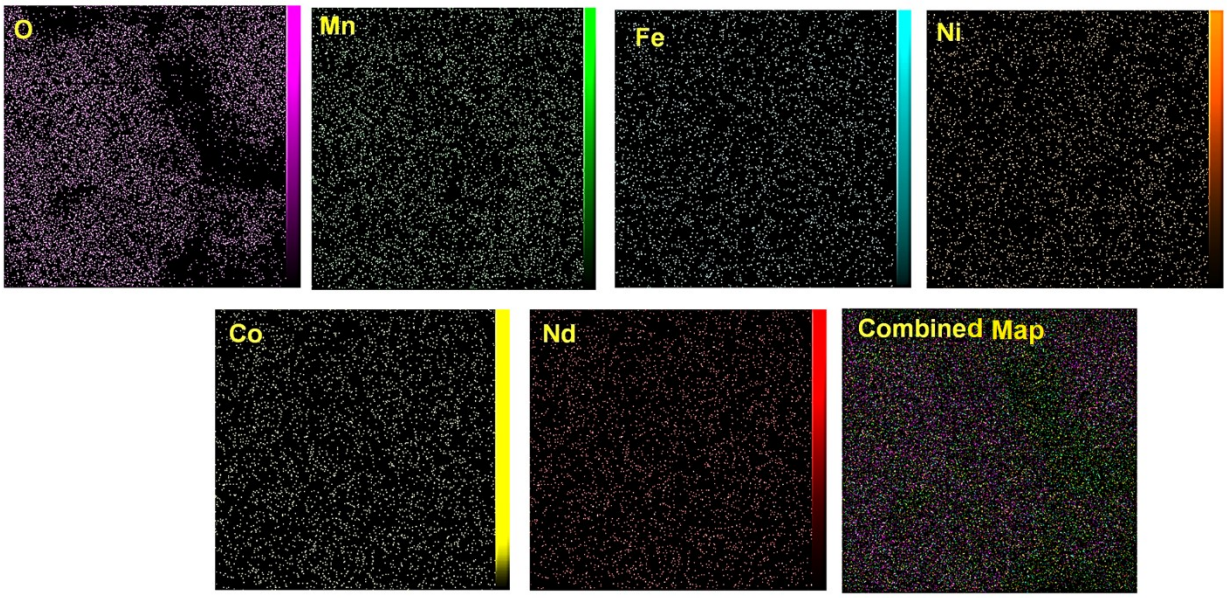

Fig. S15. FE-SEM/EDX images of the surface of modified NF with NCNFM after performing the CP test for HER.

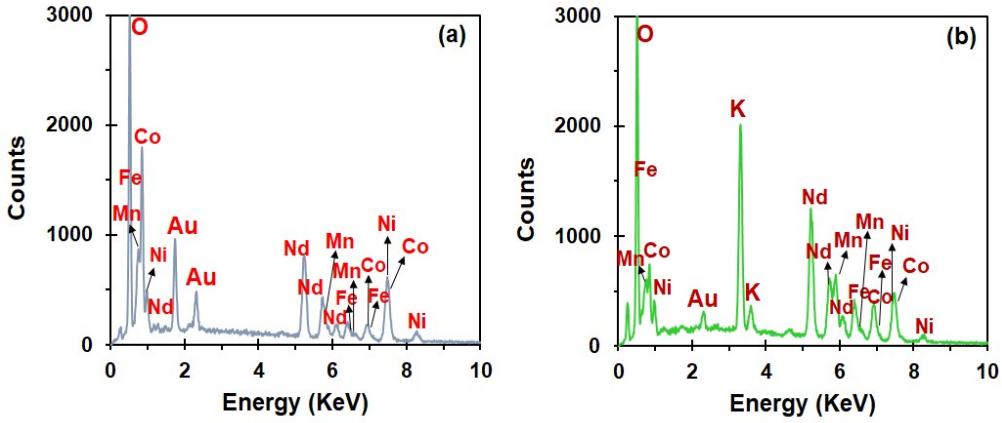

Fig. S16. EDX spectra of the surface of NCNFM/NF before (a) and after (b) the long-term stability test for HER.

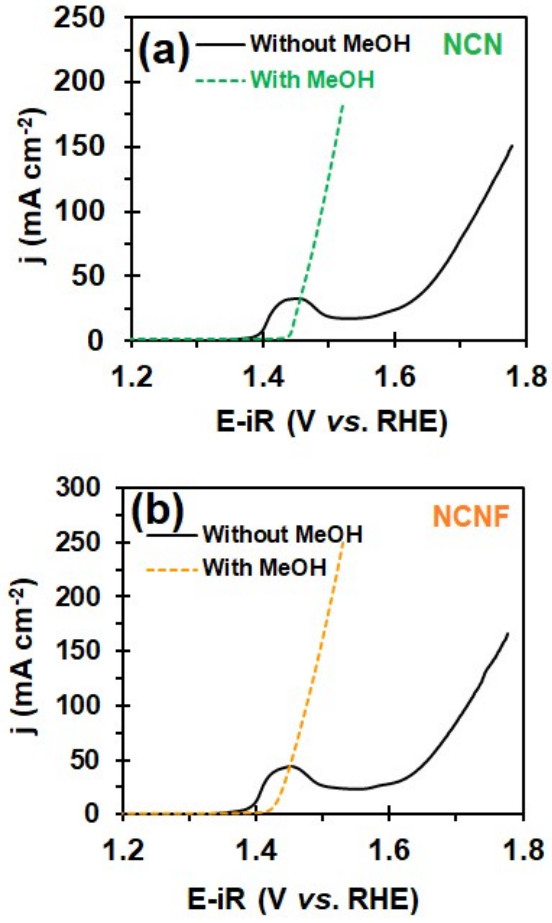

Fig. S17. iR-corrected LSV curves for MOR and OER in the presence of NCN (a), and NCNF (b) at the scan rate of 5 mV s^{-1}.

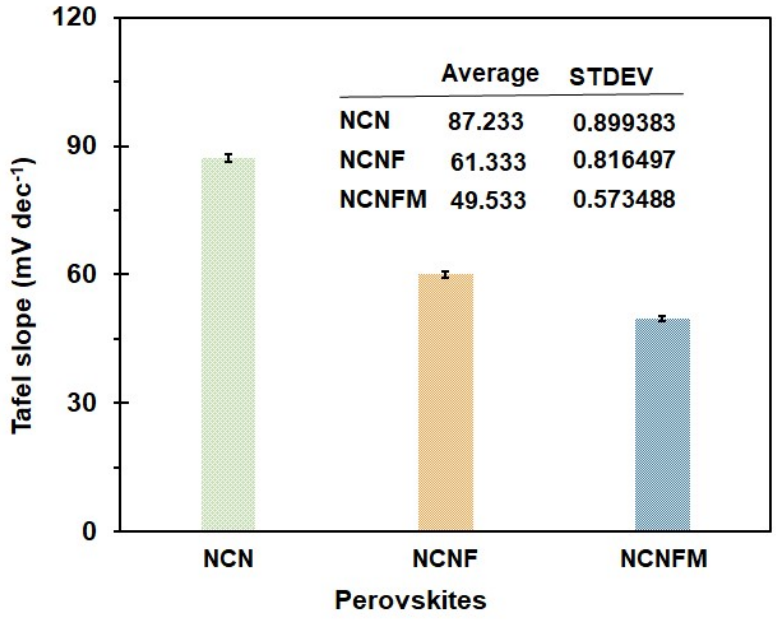

Fig. S18. Bar diagrams with error bars, showing Tafel slope values for catalysts in MOR.

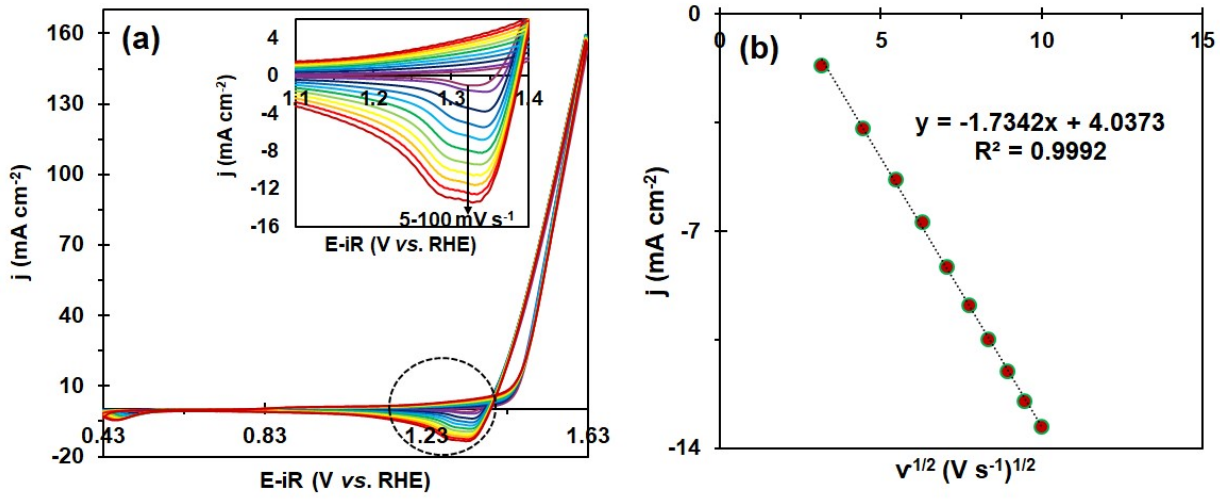

Fig. S19. CVs for NCNFM at different scan rates between 0.005-0.1 V s^{-1} in the presence of 0.5 M methanol + 1.0 M KOH solution (a), and the plot of peak current versus square root of scan rate (b).

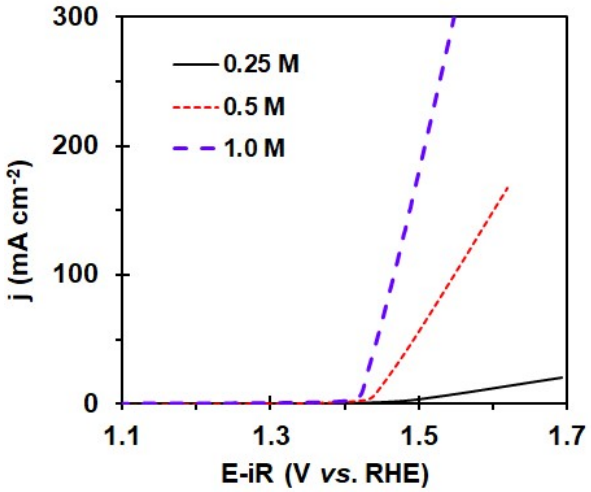

Fig. S20. iR-corrected LSV curves for NCNFM in 0.25, 0.50, and 1.0 M KOH solution with 0.50 M methanol at a scan rate of 5 mV s^{-1}.

Table S1. XRD data for the Nd-based perovskites.

Perovskite	2θ (degree), and corresponding crystal planes	Average crystallite size (nm)
NCN	23.64 (100), 33.50 (110), 41.32 (111), 48.14 (200), 54.20 (210), 59.66 (211), 70.20 (220), 79.7 (310)	71.11
NCNF	23.34 (100), 32.96(110), 40.70 (111), 47.21 (200), 53.40 (210), 59.06 (211), 69.08 (220), 78.86 (310)	36.50
NCNFM	23.10 (100), 32.84 (110), 40.22 (111), 46.95 (200), 53.22 (210), 58.86 (211), 68.90 (220)78.64 (310)	44.09

Average crystallite size was calculated upon three more intense peaks corresponding to (110), (200), and (220) crystal planes.

References:

1. Q.Luo, D.Lin, W. Zhan, W. Zhang, L. Tang, J. Luo, Z. Gao, P. Jiang, M. Wang, and L. Hao, Hexagonal perovskite $Ba_{0.9}Sr_{0.1}Co_{0.8}Fe_{0.1}Ir_{0.1}O_{3-\delta}$ as an efficient electrocatalyst towards the oxygen evolution reaction, *ACS Appl Energy Mater*., 2020, **3**,7149-7158.

2. C. C. Wang, Y. Cheng, E. Ianni, S. P. Jiang, and B. Lin, A highly active and stable $La_{0.5}Sr_{0.5}Ni_{0.4}Fe_{0.6}O_{3-\delta}$ perovskite electrocatalyst for oxygen evolution reaction in alkaline media, *Electrochim Acta*., 2017, **246**, 997-1003.

3. Z. Wang, Y. Sun, Y. Zhang, X. Wang, Q. Bai, and Y.Wang, Intrinsic electronegativity-driven design of high entropy perovskite oxide for efficient water splitting, *Ceram Int*., 2025, **51**, 19293-19301.

4. N.-I.Kim,Y.J. Sa, T. S. Yoo, S. R. Choi, R. A. Afzal, T. Choi, Y.-S. Seo, K.-S. Lee, J. Y. Hwang, and W. S. Choi, Oxygen-deficient triple perovskites as highly active and durable bifunctional electrocatalysts for oxygen electrode reactions, *Sci Adv*., 2018, **4**, eaap9360.

5. J. Sun, Z. Zhang, Y. Gong, H. Wang, R. Wang, L. Zhao, and B. He, Plasma engraved $Bi_{0.1}(Ba_{0.5}Sr_{0.5})_{0.9}Co_{0.8}Fe_{0.2}O_{3-\delta}$ perovskite for highly active and durable oxygen evolution, *Sci Rep.,* 2019, **1**, 4210.

6. J.-H. Liu, D. Yan, and S.-F. Li, Surface engineering of perovskite oxide $LaCo_{0.67}Cu_{o0.33}O_3$ for improved overall water splitting activity, *Inorg Chem*., 2025, **64**, 10533-10541.

7. S. Wu, J. Cao, Y. Zhou, J. He, J. Zhou, M. Demir, H. Yang, Z. Tong, and P. Ma, Na-modified $La(CrMnFeCoNi)_{1/5}O_3$ high entropy perovskite oxides with B-site valence fluctuations for excellent OER performance electrocatalysts, *Int J Hydrogen Energy*., 2025, **127**, 275-285.

8. J. Bian, R. Su, Y.Yao, J. Wang, J. Zhou, F. Li, Z.-L. Wang, and C. Sun, Mg doped perovskite $LaNiO_3$ nanofibers as an efficient bifunctional catalyst for rechargeable zinc–air batteries, *ACS Appl Energy Mater*., 2019, **2**, 923-931.

9. D.Bhatt, R. K. Kunchala, and B.S. Naidu, Surface engineering of perovskite oxides as a promotional approach for water-oxidation, *Surf Interfaces*., 2025, **62**, 106161.

10. X. Xu, C. Su, W. Zhou, Y. Zhu, Y. Chen, and Z. Shao, Co-doping strategy for developing perovskite oxides as highly efficient electrocatalysts for oxygen evolution reaction, *Adv Sci*., 2016, **3**, 1500187.

11. H. Qiu, B. Yuan, C. Zhao, J. Dang, C. Zhang, Q. Wang, L. Xia, H. Miao, J. Yuan, A high-entropy and low-cobalt perovskite of $La_{0.7}Sr_{0.3}Co_{0.2}Mn_{0.2}Ni_{0.2}Fe_{0.2}Al_{0.2}O_{3-x}$ for both oxygen evolution and methanol oxidation reactions, *Int J Hydrogen Energy*., 2024, **51**, 593-604.

12. Z. Zhao, X. Qu, N. Xu, and Z. Xu, Rational design of $La_{0.6}Ba_{0.4}Ti_{0.2}Fe_{0.3+x}Ni_{0.5-x}O_{3-\delta}$ (x = 0, 0.2, 0.4) perovskite oxides as bifunctional electrocatalysts for high-efficiency zinc-air batteries, *Results in Surfaces and Interfaces*., 2025, **19**, 100489.

13. G. Fu, R. Hou, L. Sun, H. Liu, Y. Wei, R. Wei, X. Meng, S. Zhang, and B. Yang, Rational regulation of high-entropy perovskite oxides through hole doping for efficient oxygen electrocatalysis, *ACS Appl Mater Interfaces*., 2025, **17**, 7860-7869.

[14] J. Bian, Z. Li, N. Li, and C. Sun, Oxygen deficient $LaMn_{0.75}Co_{0.25}O_{3-\delta}$ nanofibers as an efficient electrocatalyst for oxygen evolution reaction and zinc–air batteries, *Inorg Chem*., 2019, **58**, 8208-8214.